

Rethinking the Objectives of Vector-Quantized Tokenizers for Image Synthesis

Yuchao Gu¹, Xintao Wang², Yixiao Ge², Ying Shan², Xiaohu Qie³, Mike Zheng Shou^{1*}

¹Show Lab, National University of Singapore ²ARC Lab,³Tencent PCG

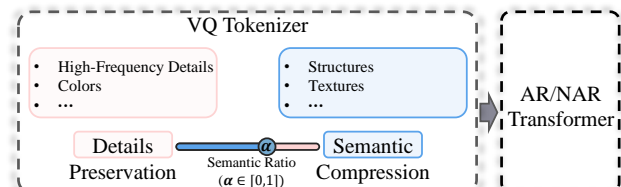
<https://github.com/TencentARC/BasicVQ-GEN>

Abstract

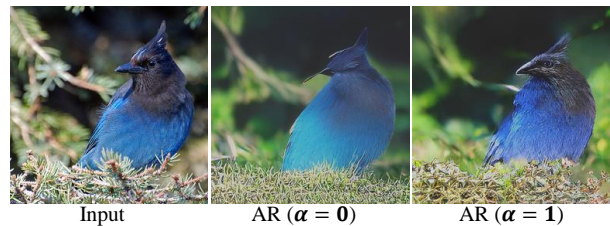
Vector-Quantized (VQ-based) generative models usually consist of two basic components, i.e., VQ tokenizers and generative transformers. Prior research focuses on improving the reconstruction fidelity of VQ tokenizers but rarely examines how the improvement in reconstruction affects the generation ability of generative transformers. In this paper, we surprisingly find that improving the reconstruction fidelity of VQ tokenizers does not necessarily improve the generation. Instead, learning to compress semantic features within VQ tokenizers significantly improves generative transformers’ ability to capture textures and structures. We thus highlight two competing objectives of VQ tokenizers for image synthesis: **semantic compression** and **details preservation**. Different from previous work that only pursues better details preservation, we propose **Semantic-Quantized GAN (SeQ-GAN)** with two learning phases to balance the two objectives. In the first phase, we propose a semantic-enhanced perceptual loss for better semantic compression. In the second phase, we fix the encoder and codebook, but enhance and finetune the decoder to achieve better details preservation. The proposed SeQ-GAN greatly improves VQ-based generative models and surpasses the GAN and Diffusion Models on both unconditional and conditional image generation. Our SeQ-GAN (364M) achieves Fréchet Inception Distance (FID) of 6.25 and Inception Score (IS) of 140.9 on 256×256 ImageNet generation, a remarkable improvement over VIT-VQGAN (714M), which obtains 11.2 FID and 97.2 IS.

1. Introduction

Recent years have witnessed remarkable progress in image synthesis. State-of-the-art results are achieved by likelihood-based generative methods, like diffusion models [13, 50], autoregressive (AR) [18, 48, 63, 64], and non-autoregressive (NAR) [8, 22] transformers. Compared to the Generative Adversarial Networks (GANs) [33, 34],



(a) Two competing objectives when optimizing VQ tokenizers.



(b) Influence of VQ tokenizers with different semantic ratio (α) on autoregressive (AR) transformers.

Figure 1. Visualization of how VQ tokenizers affect generative transformers’ generation ability.

likelihood-based generative models enjoy the benefits of stable training and better diversity. However, unlike GANs, which can generate high-resolution (e.g., 256² and 512²) images at one forward pass, likelihood-based methods usually require multiple forward passes by sequential decoding [18, 63] or iterative refinement [8, 22]. Therefore, early works [9, 26, 43], which maximize likelihood on pixel space, cannot synthesize high-resolution images due to the high computation cost and slow decoding speed.

Instead of directly modeling the underlying distribution in the pixel space, recent vector-quantized (VQ-based) generative models [55] construct a discrete latent space for generative transformers. There are two basic components in VQ-based generative models, i.e., VQ tokenizers and generative transformers. VQ tokenizers learn to quantize images into discrete codes, and then decode the codes to recover the input images, which is termed as **reconstruction**. Then, a generative transformer is trained to learn the underlying distribution in the discrete latent space constructed by the VQ tokenizer. Once trained, the generative transformer can be used to sample images from the underlying distribution, and this process is termed as **generation**. Thanks to the discrete

*Corresponding Author.



Figure 2. Visualization of our generation results. First row: LSUN- $\{\text{cat, bedroom, church}\}$. Second row: FFHQ and ImageNet.

latent space, VQ-based generative models [8, 18, 50] can easily scale up to synthesize high-resolution images without prohibitive computation cost.

The VQ tokenizer is the core component in VQ-based generative models and has received much attention. Recent VQ tokenizers [38, 49, 63, 67] try to compress more fine-grained details with finite codes to improve the reconstruction fidelity. For instance, VIT-VQGAN [63] adopts a smaller compression ratio and a larger codebook. Residual Quantization [38] recursively quantizes the feature map with a shared codebook, precisely approximating fine-grained details. Then MoVQ [67] enhances the decoder of VQ tokenizers with spatial modulation and designs a multichannel quantization with a shared codebook, achieving the finest reconstruction. With the above techniques, more fine-grained details can be compressed into VQ tokenizers, and the reconstruction fidelity is steadily improving. However, none of them have examined a fundamental question, *how the improved reconstruction of VQ tokenizers affects the generation*. Lacking such analysis is mainly because 1) they all follow an underlying assumption that “*better reconstruction, better generation*”, and 2) there is no visualization pipeline to intuitively compare generation results of various VQ tokenizers apple-to-apple.

In this paper, we first propose a visualization pipeline to examine the influence of different VQ tokenizers on generative transformers. Different from previous VQ-based generative models randomly sampling generation results, we are more curious about how generative transformers model a specific image, enabling us to check details between the reconstruction and generation side by side. The key idea of our proposed visualization pipeline is to reduce the flexibility of the sampling process by providing ground-truth context to generative transformers, which can be easily implemented with an autoregressive (AR) transformer with causal attention. The proposed visualization pipeline powers us to arrive at two important observations. 1) Improving the reconstruction fidelity of VQ tokenizers does not nec-

essarily improve the generation. 2) Learning to compress semantic features within VQ tokenizers significantly improves generative transformers’ ability to capture textures and structures. As shown in Fig. 1, the AR transformer tends to model rough color with a conventional tokenizer ($\alpha=0$) while tends to capture the structure and texture with a semantic-enhanced tokenizer ($\alpha=1$). Therefore, we highlight two competing objectives for VQ tokenizers: *semantic compression* and *details preservation*, whereas recent VQ tokenizers [38, 49, 63, 67] only pursue the latter.

To balance those two objectives, we propose **Semantic-Quantized GAN (SeQ-GAN)**, consisting of two learning phases. In the first phase, we lean to the objective of semantic compression by proposing a semantic-enhanced perceptual loss. In the second phase, we fix the encoder and codebook, but enhance and finetune the decoder to pursue better details preservation. Compared to previous VQ tokenizers, which compress fine-grained details (*e.g.*, high-frequency details, colors) into finite codes, SeQ-GAN focuses on compressing semantic features (*e.g.*, textures, structures) into codebook, but learns to restore fine-grained details by finetuning the enhanced decoder. Since training generative transformers only requires the encoder and codebook of VQ tokenizers, our decoder-only finetuning will not affect the transformer learning of structures and textures but significantly enhance the generation quality of local details.

Our main contributions are summarized as follows. (1) We rethink the common assumption “*better reconstruction, better generation*” in recent VQ tokenizers, and propose a visualization pipeline to examine the influence of different VQ tokenizers on generative transformers. (2) We point out two competing objectives in optimizing VQ tokenizers: *semantic compression* and *details preservation*. Then we introduce our solution SeQ-GAN, which balances the two objectives to achieve better generation quality. (3) Our SeQ-GAN shows remarkable improvements on conditional and unconditional image generation across both AR and NAR transformers (Examples are shown in Fig. 2).

2. Related Work

VQ-based Generative Models. The VQ-based generative model is first introduced by VQ-VAE [55], which constructs a discrete latent space by VQ tokenizers and learns the underlying latent distribution by prior models [11, 54]. Then VQGAN [18] employs perceptual loss [32, 65] and adversarial learning [21] in training VQ tokenizers, and adopts generative transformers [46] as the prior model, greatly improving the generation quality. VQ-based generative models have been applied in generation tasks, like image generation [8, 18, 63], video generations [19, 29, 61], text-to-image generations [14, 48, 50, 64], and face restorations [23, 57, 69].

Based on VQGAN [18], following works try to improve the two basic components, *i.e.*, VQ tokenizers and generative transformers, separately. To improve VQ tokenizers, VIT-VQGAN [63] proposes to quantize image features into factorized and L2-normed codes with a small compression ratio and a larger codebook, giving finer reconstruction results. Residual Quantization [38] proposes recursively quantizing the feature map using a shared codebook to precisely approximate the image feature. Following MoVQ [67] enhances the VQ tokenizer’s decoder with modulation [31], and proposes the multi-channel quantization with a shared codebook, achieving the best reconstruction results. In this paper, we argue that simply improving reconstruction fidelity does not necessarily improve the generation. Instead, we directly focus on designing VQ tokenizers for better generation quality.

Another line orthogonal to our work is improving generative transformers in VQ-based generative models. Early works adopt autoregressive (AR) transformers [18, 49, 63]. However, AR transformers suffer from low sampling speed and ignore bidirectional contexts. To tackle those problems, non-autoregressive (NAR) transformers are introduced based on different theories, like mask image modeling [3, 24] (*i.e.*, MaskGIT [8]) and discrete diffusion [2, 30] (*i.e.*, VQ-diffusion [22, 53]). In this paper, we show that adopting our SeQ-GAN as the tokenizer consistently improves the generation quality of AR and NAR transformers.

Visual Tokenizers for Generative Pretraining. Recent works in large-scale generative visual pretraining also explore the potential of the visual tokenizer. Instead of directly performing mask image modeling on pixels [24, 60], the pioneer BEiT [3] reconstructs masked patches quantized by a discrete VAE [48]. Follow-up works further strengthen the semantics of the visual tokenizer. For instance, PeCo [15] adopts contrastive perceptual loss [10, 25] when training the visual tokenizer. mc-BEiT [39] softens and re-weights the masked prediction target during visual pretraining. To further reduce the low-level representation in the visual tokenizer, iBOT [68] abandons reconstructing pixels, but updates the tokenizer online during the pretraining. BEiT-v2 [44] formulates the training objective of the visual to-

kenizer by reconstructing semantic features extracted by CLIP [45]. Different from those attempts to eliminate interference from low-level representations for visual pretraining, we focus on image synthesis and indicate the importance of semantic compression and details preservation in training VQ tokenizers for the first time.

3. Methodology

In this section, we first introduce the formulation of VQ-based generative models in Sec. 3.1. Then we present a visualization pipeline to examine the influence of different VQ tokenizers on generative transformers in Sec. 3.2. Based on the proposed pipeline, we make two critical observations and highlight two competing objectives of designing VQ tokenizers in Sec. 3.3. Finally, we propose our solution SeQ-GAN in Sec. 3.4, which balances the two objectives to achieve better generation quality.

3.1. Preliminaries

VQ-based generative models require training two basic components, *i.e.*, VQ tokenizers and generative transformers. In this section, we introduce the formulation and optimization objectives of the two components.

3.1.1 Vector-Quantized Visual Tokenizers

The role of VQ tokenizer is to compress the image into discrete latent space. Specifically, a VQ tokenizer is comprised of an encoder E , a decoder G and a codebook $\mathcal{Z} = \{z_k\}_{k=1}^K$ with K discrete codes. Given an input image $x \in \mathbb{R}^{H \times W \times 3}$, the spatial representation $\hat{z} \in \mathbb{R}^{\frac{H}{f} \times \frac{W}{f} \times n_z}$ is extracted, where n_z and f represent the latent feature’s dimension and the spatial compression ratio respectively. Then the feature at each spatial position (i, j) is quantized to the nearest code in the codebook by

$$z_{\mathbf{q}} = \mathbf{q}(\hat{z}) := \left(\arg \min_{z_k \in \mathcal{Z}} \|\hat{z}_{ij} - z_k\| \right) \in \mathbb{R}^{\frac{H}{f} \times \frac{W}{f} \times n_z}. \quad (1)$$

Then the decoder G is responsible for decoding the quantized features back to the image space. The overall reconstruction pipeline can be formulated as $\hat{x} = G(z_{\mathbf{q}}) = G(\mathbf{q}(E(x)))$. Following VQGAN [18], which employs adversarial loss (\mathcal{L}_{adv}) [21] and perceptual loss (\mathcal{L}_{per}) [32, 65] for optimizing VQ tokenizers, the overall objective can be formulated as

$$\mathcal{L}(E, G, \mathcal{Z}) = \mathcal{L}_{vq} + \mathcal{L}_{per} + \mathcal{L}_{adv}, \text{ where} \\ \mathcal{L}_{vq} = \|x - \hat{x}\|_1 + \|\text{sg}[E(x)] - z_{\mathbf{q}}\|_2^2 + \beta \|\text{sg}[z_{\mathbf{q}}] - E(x)\|_2^2. \quad (2)$$

In Eq. 2, $\text{sg}[\cdot]$ means stop-gradient and $\beta \|\text{sg}[z_{\mathbf{q}}] - E(x)\|_2^2$ is known as the commitment loss [55], where the commitment weight β is set to 0.25 following [18, 55, 63].

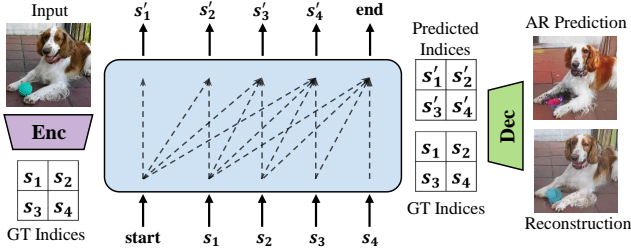


Figure 3. Visualization pipeline to examine the influence of VQ tokenizers on generative transformers.

3.1.2 Generative Transformers

Based on the trained VQ tokenizer, the image can be represented by a sequence of discrete indices. Then generative transformers are trained to model the underlying distribution in the discrete latent space. In this work, We follow the formulation of the AR transformer in VQGAN [18] and the NAR transformer in MaskGIT [8].

Autoregressive Decoding. Given an input image $x \in \mathbb{R}^{H \times W \times 3}$, we obtain its corresponding index sequence $s = [s_i]_{i=1}^N$ through the trained tokenizer, where $N = \frac{H}{f} \times \frac{W}{f}$ is the sequence length. Note that the sequence length N is related to the compression ratio f . Given context indices $s_{<i}$ and a condition c (can be class, text or null), the transformer learns to predict the next index s_i . The likelihood of the sequence s can be computed as $p(s|c) = \prod_{i \in [1, N]} p(s_i | s_{<i}, c)$. The training objective of the AR transformer is to minimize its negative log-likelihood:

$$\mathcal{L} = \mathbb{E}_{x \sim p(x)} [-\log p(s|c)]. \quad (3)$$

Non-autoregressive Decoding. The key idea of the non-autoregressive decoding is to iteratively refine the prediction from the masked indices. Specifically, given the index sequence $s = [s_i]_{i=1}^N$ from the tokenizer, a random mask is applied on s , resulting into a masked sequence s_m . Then the model is trained to predict the masked indices, which the likelihood of masked indices can be computed as $p(s|c) = \prod_{i \in [1, N], m_i=1} p(s_i | s_m, c)$, where m_i indicates whether the index is masked or not. Similar to the autoregressive decoding, the training objective is to minimize the negative log-likelihood on data using Eq. 3.

3.2. Pipeline for Visualizing VQ Generative Models

Recent VQ-based generative models examine their designs by looking into the random sampled generation results, where different sampling techniques are adopted (*e.g.*, top- p top- k sampling [28], classifier-free guidance [27], or rejection sampling [48]). Unlike previous examining random samples, we are more curious about how generative transformers model a specific image, enabling us to check details between the reconstruction and generation side by side. To achieve that goal, we propose to reduce the flexibility of the sampling process by providing ground-truth

Model	Params	rFID↓	FID↓	
			AR	NAR
baselineVQ	54.5M	3.45	16.97	13.26
+Conv×2	70.0M	3.22	17.19	13.51
+Attention×2	61.4M	2.90	17.42	14.02
+2× training	54.5M	3.28	16.19	13.26

Table 1. Comparison of VQ tokenizers on the reconstruction FID (rFID) and the generation FID on AR and NAR transformers.

(GT) contexts for predicting each index, which can be easily implemented by AR transformers.

As shown in Fig. 3, we first train a VQ tokenizer and its corresponding AR transformer. Given an image, we obtain the GT index sequence $s = [s_i]_{i=1}^N$ from the VQ tokenizer. Similar to the teacher forcing strategy [4, 58] used in training AR transformers, we feed the GT sequence s to the trained AR transformer. Because the AR transformer adopts casual attention [46], it does not directly access the GT index but accesses all GT context indices for predicting each index. Given the same context (*i.e.*, preceding GT indices), the next index prediction task is well-controlled and we can get the top-1 predicted index sequence s' within one forward pass. Then we decode the GT sequence s and the AR predicted sequence s' back to the image space by the decoder of the VQ tokenizer. In this way, we can compare the reconstruction of VQ tokenizers and the upper limit prediction of AR transformers.

3.3. Rethinking the Objectives of VQ Tokenizers

3.3.1 Observations

Based on the above visualization pipeline, we analyze the influence of VQ tokenizers on generative transformers and arrive at the following observations.

Observation 1: *Improving the reconstruction fidelity of VQ tokenizers does not necessarily improve the generation.*

We conduct a simple experiment to challenge the previous assumption that “*better reconstruction, better generation*”. We adopt a simple convolution-only VQ tokenizer as the baseline. Following VQGAN [18], we set the compression ratio $f = 16$ in Eq. 1, and each resolution level is composed of two residual blocks. Then we enhance the baseline tokenizer from three aspects: 1) Enlarging the model size: we add two residual blocks at each stage of the decoder; 2) Enhancing the model with attention: we add two interleaved dilated and block regional attention [66] at each stage of the decoder; 3) Employing a longer training schedule: we train the VQ tokenizer with $2 \times$ iterations. Both the VQ tokenizers and the generative transformers are trained on 256×256 ImageNet for 500,000 iterations. More experimental details are provided in Sec. 6.1.

The reconstruction results of different tokenizers and their corresponding generation results are summarized in Table. 1. Compared to the baseline tokenizer, different

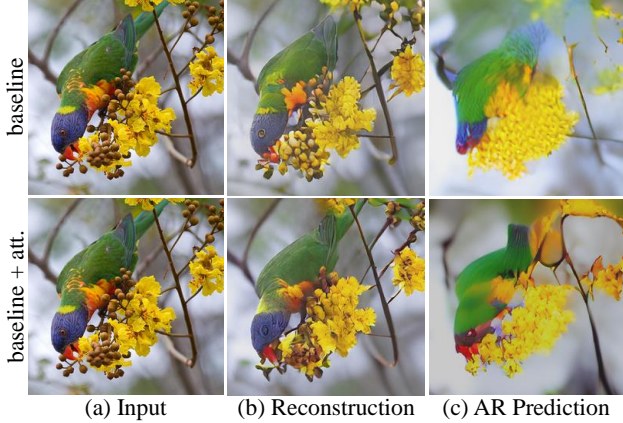


Figure 4. Comparison between the baseline tokenizer and its attention-enhanced variant on reconstructions and AR predictions.

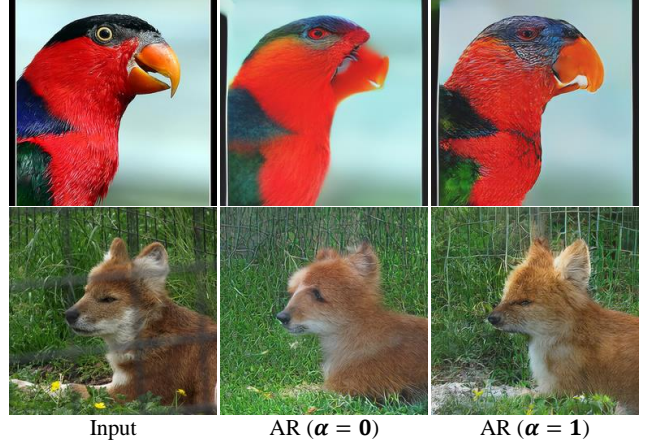
enhanced tokenizers improve the reconstruction fidelity. Among them, adding attention achieves the best reconstruction fidelity, improving about 0.55 reconstruction FID (rFID) over the baseline tokenizer. However, regarding the generation quality, compared to the baseline tokenizer, the enhanced tokenizers only maintain a similar or even worse generation FID on both AR and NAR transformers, in spite of their better rFID. The results contradict the previous common assumption and motivates us to examine the influence of different tokenizer designs on generation carefully.

We then adopt the proposed visualization pipeline (in Sec. 3.2) to pairwise compare the reconstruction and generation results between the baseline tokenizer (1st row) and its attention-enhanced variant (2nd row). As shown in Fig. 4, despite the attention-enhanced variant achieves a more consistent reconstruction (e.g., color and high-frequency details) to the input, the AR transformer cannot model such details but only captures a rough color of the main object. The visualization shows a large discrepancy between the reconstruction and generation. Therefore, simply improving the reconstruction fidelity of VQ tokenizers cannot benefit the generation quality.

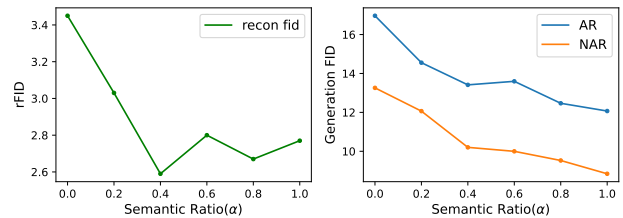
Observation 2: *Semantic compression within VQ tokenizers benefits the generative transformer.*

Since there is a large discrepancy between the tokenizers’ reconstruction and the AR transformer’s prediction, compressing more fine-grained details within the tokenizer cannot always benefit the generation. This observation leads us to explore the role of semantics in VQ tokenizers for generation quality, which has been proven to be useful in large-scale generative pretraining [39, 44, 68]. Unlike generative pretraining that gradually abandons the low-level representation in their tokenizers to pursue semantic representation, low-level representation is undoubtedly important for image synthesis. Therefore, we need to find a method to balance the low-level details and semantic information compressed in VQ tokenizers.

Motivated by previous research of perceptual loss [32],



(a) Visualization of the AR predicted results when training upon VQ tokenizers of different semantic ratio (α).



(b) Reconstruction FID and generation FID with different semantic ratio (α) in optimizing VQ tokenizers.

Figure 5. Influence of the semantic ratio α in VQ tokenizers on generation quality.

we modify the perceptual loss to control the semantic ratio. Specifically, given an input and a reference image, we extract their activation features \hat{y}^l and y^l from a pre-trained VGG [52] network. For each layer l , the feature is of shape $H_l \times W_l \times C_l$. Then, the perceptual loss can be calculated as $\mathcal{L}_{per} = \sum_l \frac{1}{H_l W_l C_l} \|\hat{y}^l - y^l\|_2^2$. To preserve details, perceptual loss [65] used in previous VQ tokenizers adopts the features from both the shallow and high layers, which we denote as L_{per}^{low} in this paper. To better compress semantic information during reconstruction, we propose a semantic-enhanced perceptual loss L_{per}^{sem} , which removes the features from shallow layers and further includes the logit feature (i.e., feature before softmax classifier). The layers l to extract features can be summarized as

- \mathcal{L}_{per}^{low} : $l \in \{\text{relu}\{1.2, 2.2, 3.3, 4.3, 5.3\}\}$,
- \mathcal{L}_{per}^{sem} : $l \in \{\text{relu5.3, logit}\}$.

We re-weight the two perceptual losses to control the proportion between the details and semantic information by

$$\mathcal{L}_{per}^\alpha = \alpha \mathcal{L}_{per}^{sem} + (1 - \alpha) \mathcal{L}_{per}^{low}, \quad (4)$$

where $\alpha \in [0, 1]$ is the semantic ratio.

We then investigate the influence of tokenizers with different semantic ratios α on generation quality. Fig. 5(b) shows that adding \mathcal{L}_{per}^{sem} into the reconstruction objective improves the reconstruction FID (rFID). The best rFID is achieved when $\alpha = 0.4$. And, the generation FID consistently improves with the increase of the semantic ratio α

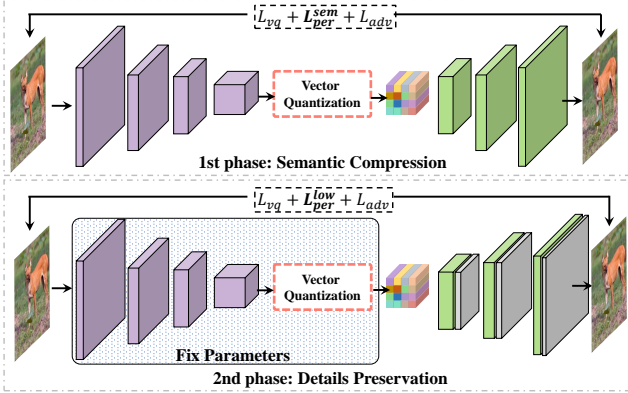


Figure 6. Pipeline of the two-phase learning in SeQ-GAN.

VQ tokenizers. As Fig. 5(a) and Fig. 1(b) shown, with the semantic-enhanced VQ tokenizer ($\alpha = 1$), the AR transformer can capture more overall structures and textures than the baseline tokenizer ($\alpha = 0$).

3.3.2 Discussion

Based on the above observations, we rethink the optimizing objectives of VQ tokenizers in VQ-based generative models. One objective is to quantize the image with finite codes and reconstruct the quantized code back to image space without losing much perceptual fidelity, which has been extensively researched in previous works [38, 63, 67]. But different from tokenizers [36, 51] in Natural Language Processing (NLP), which are naturally discrete and semantic meaningful, the VQ tokenizer contains little semantics [39] and is sensitive to invisible low-level changes (evidence is shown in Sec. 6.2). Such a latent space probably poses difficulties for generative transformers to model, since transformers are better at capturing long-range dependency [16]. Therefore, VQ tokenizers should learn to semantically compress the image for generative transformer training. Note that different from the definition of semantics in generative pretraining [44, 68], which totally eliminate the low-level representation, the semantics in VQ-based generative models refer to the structures and textures, and the details refer to colors and high-frequency details. In this paper, we argue that both semantic compression and details preservation should be considered when designing VQ tokenizers for image synthesis.

3.4. Our Solution: SeQ-GAN

To achieve better generation quality, we propose the **Semantic-Quantized GAN (SeQ-GAN)** as the VQ tokenizer in VQ-based generative models, balancing the objectives of semantic compression and details preservation.

As shown in Fig. 6, SeQ-GAN divides the tokenizer learning into two phases. In the first phase, we pursue semantic compression, which adopts the proposed semantic-enhanced perceptual loss $\mathcal{L}_{per}^{\alpha=1}$ in Eq. 4. However, the VQ

Model	Datset	Latent Size	Codebook K	Usage	rFID
VQGAN [18]	FFHQ	16×16	1024	42%	4.42
VIT-VQGAN [63]		32×32	8192	-	3.13
RQ-VAE [38]		$16 \times 16 \times 4$	2048	-	3.88
MoVQ [67]		$16 \times 16 \times 4$	1024	-	2.26
SeQ-GAN (Ours)		16×16	1024	100%	3.12
VQGAN [18]	ImageNet	16×16	1024	44%	7.94
VQGAN [18]		16×16	16384	5.9%	4.98
VIT-VQGAN [63]		32×32	8192	96%	1.28
RQ-VAE [38]		$8 \times 8 \times 16$	16384	-	1.83
MoVQ [67]		$16 \times 16 \times 4$	1024	-	1.12
SeQ-GAN (Ours)		16×16	1024	100%	1.99

Table 2. Quantitative reconstruction results on ImageNet [12] and FFHQ [33] validation set. K means the codebook size.

tokenizer learned to make semantic compression will lose some fidelity of colors and high-frequency details. Motivated by image restoration [56], those details can be restored with a powerful decoder. Therefore, we enhance the decoder with interleaved block regional and dilated attention [66]. We fix the encoder and codebook of the tokenizer, but finetune the enhanced decoder with $\mathcal{L}_{per}^{\alpha=0}$ to achieve better details preservation. Since training generative transformers only requires the encoder and codebook of VQ tokenizers, our decoder-only finetuning will not affect the transformer learning of structures and textures, but significantly enhance the generation quality of local details.

When training our SeQ-GAN, we observe the problem of low codebook usages, which also exists in previous VQGAN [18]. A similar problem (*i.e.*, empty cluster) has been observed in self-supervised representation learning [1, 6, 7, 40]. A quick fix to this problem contains offline clustering [1, 6] or entropy regularization [7, 40]. In this work, we adopt entropy regularization to solve the problem of low codebook usages as default. Specifically, given the feature before quantization $\hat{z} \in \mathbb{R}^{N \times n_z}$, we aim to map \hat{z} to the codebook feature $\mathcal{Z} = \{z_k\}_{k=1}^K$. Denote the matrix $\mathcal{D} \in \mathbb{R}^{N \times K}$ as the L2 distance between each feature \hat{z}_i and each code entry z_k , we normalize it by softmax $\mathcal{D}_{i,k} = \frac{\exp(-\mathcal{D}_{i,k})}{\sum_{k=1}^K \exp(-\mathcal{D}_{i,k})}$. Then we average \mathcal{D} along the spatial size by $\bar{\mathcal{D}}_k = \frac{1}{N} \sum_{i=1}^N \mathcal{D}_{i,k}$, where $\bar{\mathcal{D}} \in \mathbb{R}^K$ can be interpreted as a soft codebook usage. To increase the codebook usage, we encourage a smoother $\bar{\mathcal{D}}$, which achieved by penalizing the entropy $H(\bar{\mathcal{D}}) = -\sum_k \bar{\mathcal{D}}_k \log \bar{\mathcal{D}}_k$. And we update the optimization objective in Eq. 2 to $\mathcal{L}_{vq'} = \mathcal{L}_{vq} + \gamma H(\bar{\mathcal{D}})$, where we fix $\gamma = 0.01$ in our experiments.

Model	Params	steps	FFHQ	Church	Cat	Bedroom
BigGAN [5]	164M	1	12.4	-	-	-
StyleGAN2 [34]	30M	1	3.8	3.86	7.25	2.35
ADM [13]	552M	1000	-	-	5.57	1.90
DDPM [26]	114M [†] /256M [‡]	1000	-	7.89 [†]	19.75 [†]	4.90 [‡]
DCT [41]	473M [†] /448M [‡]	>1024	13.06 [†]	7.56 [‡]	-	6.40 [‡]
VQGAN [18]	72.1M + 801M	256	11.4	7.81	17.31	6.35
ImageBART [17]	-	-	9.57	7.32	15.09	5.51
VIT-VQGAN [63]	64M + 1697M	1024	5.3	-	-	-
RQ-VAE [38]	100M + 370M [†] /650M [‡]	256	10.38 [†]	7.45 [†]	8.64 [‡]	3.04 [‡]
MoVQ + AR [67]	82.7M + 307M	1024	8.52	-	-	-
MoVQ + NAR [67]	82.7M + 307M	12	8.78	-	-	-
SeQ-GAN + AR (Ours)	57.9M + 171M	256	-	2.45	3.61	1.44
SeQ-GAN + NAR (Ours)	57.9M + 171M	12	3.62	2.25	4.60	2.05

Table 3. Quantitative comparison of unconditional image generation on FFHQ [33] and LSUN [62]-{Church, Cat, Bedroom}. We omit the auto-regressive (AR) transformer result on FFHQ, because it has a severe overfitting, consistent with the finding in RQ-VAE [38].

4. Experiments

4.1. Image Quantization

We train the SeQ-GAN on ImageNet [12], FFHQ [33] and LSUN [62], separately. In the first phase of tokenizer learning, we train the SeQ-GAN on ImageNet and FFHQ with Adam [35] optimizer with a learning rate of 1e-4 for 500,000 iterations. For LSUN [62]-{cat, bedroom, church}, we follow RQ-VAE [38] to use the pretrained SeQ-GAN on ImageNet and finetune for one epoch on each dataset. In the second phase, we finetune the enhanced decoder of SeQ-GAN on ImageNet, FFHQ and LSUN for 200,000 iterations with a learning rate of 5e-4. The detailed settings are shown in Sec. 6.1.

The results are summarized in Table. 2. Since VIT-VQGAN [63], RQ-VAE [38] and MoVQ [67] target at compressing more fine-grained details for improving the reconstruction fidelity, they usually require a larger latent size. Our SeQ-GAN does not simply pursue the reconstruction fidelity, but aims to optimize for better generation quality. Therefore, SeQ-GAN does not achieve the best reconstruction fidelity. However, compared to VQGAN [18], with the same latent size and codebook size, SeQ-GAN still has a large improvement in rFID and codebook usage.

4.2. Unconditional Image Generation

On top of the SeQ-GAN, we train AR and NAR transformers for unconditional generation on FFHQ [33] and LSUN [62]. All models are trained for 500,000 iterations with the Adam optimizer with a learning rate of 1e-4. Detailed hyperparameters are listed in Sec. 6.1.

From the results in Table. 3, previous state-of-the-art results are achieved by continuous diffusion model ADM [13] and StyleGAN2 [34]. VQ-based generative models largely lag behind. But when adopting our SeQ-GAN as the VQ

Model	Params	Steps	FID	IS
BigGAN-Deep [5]	160M	1	6.95	198.2
DCT [41]	738M	>1024	36.51	-
Improved DDPM [42]	280M	250	12.26	-
ADM [13]	554M	250	10.94	101.0
VQ-VAE-2 [49]	13.5B	5120	31.11	~45
VQGAN [18]	1.4B	256	15.78	78.3
VIT-VQGAN [63]	714M	256	11.20	97.2
VIT-VQGAN [63]	1.7B	1024	4.17	175.1
RQ-VAE [38]	1.4B	1024	8.71	119.0
MoVQ + AR [67]	389M	1024	7.13	138.3
SeQ-GAN + AR	229M	256	7.55	121.3
SeQ-GAN + AR	364M	256	6.25	140.9
VQ-Diffusion [22]	370M	100	11.89	-
MaskGIT [8]	227M	8	6.18	182.1
MoVQ + NAR [67]	389M	12	7.22	130.1
SeQ-GAN + NAR	229M	12	4.99	189.1
SeQ-GAN + NAR	364M	12	4.55	200.4

Table 4. FID and Inception Score (IS) comparison of conditional image generation on ImageNet [12].

tokenizer, the AR/NAR transformer with 171M parameters achieve strong performance over VIT-VQGAN [63], RQ-VAE [38] and MoVQ [67]. Moreover, SeQ-GAN makes VQ-based generative models first surpass ADM and StyleGAN2 on FFHQ and LSUN.

4.3. Conditional Image Generation

We train AR and NAR transformers with our SeQ-GAN tokenizer on 256×256 ImageNet generation. To directly compare to VIT-VQGAN [63] and MaskGIT [8], the model is trained with 300 epochs with a learning rate of 1e-4. Other training setting are in the Sec. 6.1.

Model	Dim \mathcal{Z}	K	Usage	rFID	AR	NAR
VQGAN	256	1024	43.5%	4.07	17.19	14.58
+ F&N	32	8192	99.7%	2.93	24.91	-
+ K-means	256	1024	100%	3.54	16.84	15.02
+ $H(\hat{\mathcal{D}})$	256	1024	100%	3.45	16.97	13.26

Table 5. Ablation of codebook regularization. We run the VQGAN [18] as baseline. *F&N* means the factorized and L2-normed codebook in VIT-VQGAN [63]. K means the codebook size.

Loss	relu1_2	relu2_2	relu3_3	relu4_3	relu5_3	logit	rFID	AR	NAR
\mathcal{L}_{per}^{low}	✓	✓	✓	✓	✓		3.45	16.97	13.26
A	✓	✓	✓	✓	✓	✓	3.01	15.19	11.78
B		✓	✓	✓	✓	✓	2.93	14.47	11.58
C			✓	✓	✓	✓	2.81	14.08	10.52
D				✓	✓	✓	2.62	13.34	9.56
\mathcal{L}_{per}^{sem}					✓	✓	2.77	12.07	8.84
E						✓	4.65	17.88	14.00

Table 6. Ablation of semantic-enhanced perceptual loss designs.

The results are summarized in Table. 4. our SeQ-GAN+AR (364M, 256 sample steps) achieves FID of 6.25 and IS of 140.9, a remarkable improvement over VIT-VQGAN [63] (714M, 256 sample steps), which obtains 11.2 FID and 97.2 IS. Compared to the non-autoregressive (NAR) transformer MaskGIT [8], which obtains 6.18 FID, our SeQ-GAN+NAR achieves a better 4.99 FID with the same sampling step and a similar model size. And compared to MoVQ+NAR (389M, 12 sample steps), obtaining 7.22 FID and 130.1 IS, SeQ-GAN+NAR (364M, 12 sample steps) achieving a much better performance of 4.55 FID and 200.4 IS. With the same model size, we find the NAR transformer shows better performance and fewer sample steps than the AR transformer on conditional image synthesis.

4.4. Ablation

Codebook regularization. We ablate the strategy for increasing codebook usages in the baseline setting (one-phase training with $\mathcal{L}_{per}^{\alpha=0}$). As shown in Table. 5, although the factorized and L2-normed codebook in VIT-VQGAN can largely enhance the reconstruction fidelity, its large codebook size results in a suboptimal performance on the AR transformer. Moreover, optimizing the NAR transformer on a large codebook size is unstable. Compared to the offline K-means clustering used in previous codebook learning [37], the entropy regularization used in our paper achieves a better reconstruction and generation performance.

Design of semantic-enhanced perceptual loss. From the result in Table. 6, the baseline is the \mathcal{L}_{per}^{low} , which adopts all five layers to compute perceptual loss. Adding the logit feature improves both the rFID and generation FID. Variant-D achieves the best rFID while \mathcal{L}_{per}^{sem} achieves the best gen-



(a) Influence of the 2nd-phase tokenizer learning on perceptual quality.

Model	SeQ-GAN	ImageNet	FFHQ	Church	Cat	Bedroom
AR	1st phase	7.83	-	3.49	4.73	2.15
	2nd phase	7.55	-	2.45	3.61	1.44
NAR	1st phase	5.31	3.89	3.41	5.22	2.88
	2nd phase	4.99	3.62	2.25	4.60	2.05

(b) Influence of the phase-2 tokenizer learning on FID.

Figure 7. Ablation for the influence of the 2nd-phase tokenizer learning on generation.

eration FID, which also verifies the reconstruction fidelity does not necessarily connect to the generation performance. With removing more shallow layers, the generation quality consistently improves, demonstrating the importance of semantics when optimizing VQ tokenizers for generation. Adopting the logit feature (variant-E) without spatial feature results in significantly worse performance. Although removing different perceptual layers can also adjust the balance between details and semantics, it usually involves the extensive parameter tunings to match the loss scale. Instead, we fix the \mathcal{L}_{per}^{low} and the \mathcal{L}_{per}^{sem} , and simply tuning the semantic ratio α in Eq. 4 to achieve that goal.

Influence of the second phase tokenizer learning. Because SeQ-GAN is trained with semantic-enhanced perceptual loss $\mathcal{L}_{per}^{\alpha=1}$ in the 1st phase, it loses some fidelity in color and high-frequency details. By finetuning the enhanced decoder in the 2nd phase, those details can be preserved for generation. From the visualization in Fig. 7(a), the color distortion (*e.g.*, windows) can be restored with the 2nd phase learning. Also, from the results in Fig. 7(b), the 2nd phase learning improves the generation FID consistently. Note that enhancing the decoder to compress more fine-grained details into the codebook degrades the generation performance (see Table. 1), which shows the decoder-only finetuning in our SeQ-GAN can better balance the objectives of semantic compression and details preservation.

5. Conclusion

This work examines a fundamental question in VQ-based generative models, “how the improved reconstruction

of VQ tokenizers affects the generation”. To answer this question, we introduce a visualization pipeline to examine the influence of different tokenizers on AR transformers. Based on this pipeline, we find both semantic compression and details preservation should be considered in optimizing VQ tokenizers, in which previous works only focus on the latter. Based on this finding, we propose a simple solution SeQ-GAN, which achieves remarkable improvement over existing VQ-based generative models on image synthesis.

References

- [1] Yuki Markus Asano, Christian Rupprecht, and Andrea Vedaldi. Self-labelling via simultaneous clustering and representation learning. *arXiv preprint arXiv:1911.05371*, 2019. 6
- [2] Jacob Austin, Daniel D Johnson, Jonathan Ho, Daniel Tarlow, and Rianne van den Berg. Structured denoising diffusion models in discrete state-spaces. *NeurIPS*, 34:17981–17993, 2021. 3
- [3] Hangbo Bao, Li Dong, and Furu Wei. Beit: Bert pre-training of image transformers. *arXiv preprint arXiv:2106.08254*, 2021. 3
- [4] Samy Bengio, Oriol Vinyals, Navdeep Jaitly, and Noam Shazeer. Scheduled sampling for sequence prediction with recurrent neural networks. *NeurIPS*, 28, 2015. 4
- [5] Andrew Brock, Jeff Donahue, and Karen Simonyan. Large scale gan training for high fidelity natural image synthesis. *arXiv preprint arXiv:1809.11096*, 2018. 7, 15, 17, 18, 19
- [6] Mathilde Caron, Piotr Bojanowski, Armand Joulin, and Matthijs Douze. Deep clustering for unsupervised learning of visual features. In *ECCV*, pages 132–149, 2018. 6
- [7] Mathilde Caron, Ishan Misra, Julien Mairal, Priya Goyal, Piotr Bojanowski, and Armand Joulin. Unsupervised learning of visual features by contrasting cluster assignments. *NeurIPS*, 33:9912–9924, 2020. 6
- [8] Huiwen Chang, Han Zhang, Lu Jiang, Ce Liu, and William T Freeman. Maskgit: Masked generative image transformer. In *CVPR*, pages 11315–11325, 2022. 1, 2, 3, 4, 7, 8, 12, 15, 17, 18, 19
- [9] Mark Chen, Alec Radford, Rewon Child, Jeffrey Wu, Heewoo Jun, David Luan, and Ilya Sutskever. Generative pre-training from pixels. In *ICML*, pages 1691–1703. PMLR, 2020. 1
- [10] Xinlei Chen, Haoqi Fan, Ross Girshick, and Kaiming He. Improved baselines with momentum contrastive learning. *arXiv preprint arXiv:2003.04297*, 2020. 3
- [11] Xi Chen, Nikhil Mishra, Mostafa Rohaninejad, and Pieter Abbeel. Pixelsnail: An improved autoregressive generative model. In *ICML*, pages 864–872. PMLR, 2018. 3
- [12] Jia Deng, Wei Dong, Richard Socher, Li-Jia Li, Kai Li, and Li Fei-Fei. Imagenet: A large-scale hierarchical image database. In *CVPR*, pages 248–255. Ieee, 2009. 6, 7, 12, 13, 17, 18, 19
- [13] Prafulla Dhariwal and Alexander Nichol. Diffusion models beat gans on image synthesis. *NeurIPS*, 34:8780–8794, 2021. 1, 7
- [14] Ming Ding, Zhuoyi Yang, Wenyi Hong, Wendi Zheng, Chang Zhou, Da Yin, Junyang Lin, Xu Zou, Zhou Shao, Hongxia Yang, et al. Cogview: Mastering text-to-image generation via transformers. *NeurIPS*, 34:19822–19835, 2021. 3
- [15] Xiaoyi Dong, Jianmin Bao, Ting Zhang, Dongdong Chen, Weiming Zhang, Lu Yuan, Dong Chen, Fang Wen, and Nenghai Yu. Peco: Perceptual codebook for bert pre-training of vision transformers. *arXiv preprint arXiv:2111.12710*, 2021. 3
- [16] Alexey Dosovitskiy, Lucas Beyer, Alexander Kolesnikov, Dirk Weissenborn, Xiaohua Zhai, Thomas Unterthiner, Mostafa Dehghani, Matthias Minderer, Georg Heigold, Sylvain Gelly, et al. An image is worth 16x16 words: Transformers for image recognition at scale. *arXiv preprint arXiv:2010.11929*, 2020. 6
- [17] Patrick Esser, Robin Rombach, Andreas Blattmann, and Bjorn Ommer. Imagebart: Bidirectional context with multinomial diffusion for autoregressive image synthesis. *NeurIPS*, 34:3518–3532, 2021. 7
- [18] Patrick Esser, Robin Rombach, and Bjorn Ommer. Taming transformers for high-resolution image synthesis. In *CVPR*, pages 12873–12883, 2021. 1, 2, 3, 4, 6, 7, 8, 12, 15, 17, 18, 19
- [19] Songwei Ge, Thomas Hayes, Harry Yang, Xi Yin, Guan Pang, David Jacobs, Jia-Bin Huang, and Devi Parikh. Long video generation with time-agnostic vqgan and time-sensitive transformer. *arXiv preprint arXiv:2204.03638*, 2022. 3
- [20] Robert Geirhos, Patricia Rubisch, Claudio Michaelis, Matthias Bethge, Felix A Wichmann, and Wieland Brendel. Imagenet-trained cnns are biased towards texture; increasing shape bias improves accuracy and robustness. *arXiv preprint arXiv:1811.12231*, 2018. 16
- [21] Ian Goodfellow, Jean Pouget-Abadie, Mehdi Mirza, Bing Xu, David Warde-Farley, Sherjil Ozair, Aaron Courville, and Yoshua Bengio. Generative adversarial networks. *Communications of the ACM*, 63(11):139–144, 2020. 3
- [22] Shuyang Gu, Dong Chen, Jianmin Bao, Fang Wen, Bo Zhang, Dongdong Chen, Lu Yuan, and Baining Guo. Vector quantized diffusion model for text-to-image synthesis. In *CVPR*, pages 10696–10706, 2022. 1, 3, 7
- [23] Yuchao Gu, Xintao Wang, Liangbin Xie, Chao Dong, Gen Li, Ying Shan, and Ming-Ming Cheng. Vqfr: Blind face restoration with vector-quantized dictionary and parallel decoder. *arXiv preprint arXiv:2205.06803*, 2022. 3
- [24] Kaiming He, Xinlei Chen, Saining Xie, Yanghao Li, Piotr Dollár, and Ross Girshick. Masked autoencoders are scalable vision learners. In *CVPR*, pages 16000–16009, 2022. 3
- [25] Kaiming He, Haoqi Fan, Yuxin Wu, Saining Xie, and Ross Girshick. Momentum contrast for unsupervised visual representation learning. In *CVPR*, pages 9729–9738, 2020. 3
- [26] Jonathan Ho, Ajay Jain, and Pieter Abbeel. Denoising diffusion probabilistic models. *NeurIPS*, 33:6840–6851, 2020. 1, 7
- [27] Jonathan Ho and Tim Salimans. Classifier-free diffusion guidance. *arXiv preprint arXiv:2207.12598*, 2022. 4, 12, 16

- [28] Ari Holtzman, Jan Buys, Li Du, Maxwell Forbes, and Yejin Choi. The curious case of neural text degeneration. *arXiv preprint arXiv:1904.09751*, 2019. 4, 12
- [29] Wenyi Hong, Ming Ding, Wendi Zheng, Xinghan Liu, and Jie Tang. Cogvideo: Large-scale pretraining for text-to-video generation via transformers. *arXiv preprint arXiv:2205.15868*, 2022. 3
- [30] Emiel Hoogeboom, Didrik Nielsen, Priyank Jaini, Patrick Forré, and Max Welling. Argmax flows and multinomial diffusion: Towards non-autoregressive language models. 2021. 3
- [31] Xun Huang and Serge Belongie. Arbitrary style transfer in real-time with adaptive instance normalization. In *ICCV*, pages 1501–1510, 2017. 3
- [32] Justin Johnson, Alexandre Alahi, and Li Fei-Fei. Perceptual losses for real-time style transfer and super-resolution. In *ECCV*, pages 694–711. Springer, 2016. 3, 5
- [33] Tero Karras, Samuli Laine, and Timo Aila. A style-based generator architecture for generative adversarial networks. In *CVPR*, pages 4401–4410, 2019. 1, 6, 7, 13, 16
- [34] Tero Karras, Samuli Laine, Miika Aittala, Janne Hellsten, Jaakko Lehtinen, and Timo Aila. Analyzing and improving the image quality of stylegan. In *CVPR*, pages 8110–8119, 2020. 1, 7, 12
- [35] Diederik P Kingma and Jimmy Ba. Adam: A method for stochastic optimization. *arXiv preprint arXiv:1412.6980*, 2014. 7
- [36] Taku Kudo and John Richardson. Sentencepiece: A simple and language independent subword tokenizer and detokenizer for neural text processing. *arXiv preprint arXiv:1808.06226*, 2018. 6
- [37] Adrian Łańcucki, Jan Chorowski, Guillaume Sanchez, Ricardo Marxer, Nanxin Chen, Hans JGA Dolfing, Sameer Khurana, Tanel Alumäe, and Antoine Laurent. Robust training of vector quantized bottleneck models. In *IEEE IJCNN*, pages 1–7. IEEE, 2020. 8
- [38] Doyup Lee, Chihyeon Kim, Saehoon Kim, Minsu Cho, and Wook-Shin Han. Autoregressive image generation using residual quantization. In *CVPR*, pages 11523–11532, 2022. 2, 3, 6, 7
- [39] Xiaotong Li, Yixiao Ge, Kun Yi, Zixuan Hu, Ying Shan, and Ling-Yu Duan. mc-beit: Multi-choice discretization for image bert pre-training. *arXiv preprint arXiv:2203.15371*, 2022. 3, 5, 6, 12
- [40] Yunfan Li, Peng Hu, Zitao Liu, Dezhong Peng, Joey Tianyi Zhou, and Xi Peng. Contrastive clustering. In *AAAI*, volume 35, pages 8547–8555, 2021. 6
- [41] Charlie Nash, Jacob Menick, Sander Dieleman, and Peter W Battaglia. Generating images with sparse representations. *arXiv preprint arXiv:2103.03841*, 2021. 7
- [42] Alexander Quinn Nichol and Prafulla Dhariwal. Improved denoising diffusion probabilistic models. In *ICML*, pages 8162–8171. PMLR, 2021. 7
- [43] Niki Parmar, Ashish Vaswani, Jakob Uszkoreit, Lukasz Kaiser, Noam Shazeer, Alexander Ku, and Dustin Tran. Image transformer. In *ICML*, pages 4055–4064. PMLR, 2018. 1
- [44] Zhiliang Peng, Li Dong, Hangbo Bao, Qixiang Ye, and Furu Wei. Beit v2: Masked image modeling with vector-quantized visual tokenizers. *arXiv preprint arXiv:2208.06366*, 2022. 3, 5, 6
- [45] Alec Radford, Jong Wook Kim, Chris Hallacy, Aditya Ramesh, Gabriel Goh, Sandhini Agarwal, Girish Sastry, Amanda Askell, Pamela Mishkin, Jack Clark, et al. Learning transferable visual models from natural language supervision. In *ICML*, pages 8748–8763. PMLR, 2021. 3
- [46] Alec Radford, Jeffrey Wu, Rewon Child, David Luan, Dario Amodei, Ilya Sutskever, et al. Language models are unsupervised multitask learners. *OpenAI blog*, 1(8):9, 2019. 3, 4
- [47] Prajit Ramachandran, Barret Zoph, and Quoc V Le. Searching for activation functions. *arXiv preprint arXiv:1710.05941*, 2017. 12
- [48] Aditya Ramesh, Mikhail Pavlov, Gabriel Goh, Scott Gray, Chelsea Voss, Alec Radford, Mark Chen, and Ilya Sutskever. Zero-shot text-to-image generation. In *ICML*, pages 8821–8831. PMLR, 2021. 1, 3, 4, 12, 16
- [49] Ali Razavi, Aaron Van den Oord, and Oriol Vinyals. Generating diverse high-fidelity images with vq-vae-2. *NeurIPS*, 32, 2019. 2, 3, 7
- [50] Robin Rombach, Andreas Blattmann, Dominik Lorenz, Patrick Esser, and Björn Ommer. High-resolution image synthesis with latent diffusion models. In *CVPR*, pages 10684–10695, 2022. 1, 2, 3
- [51] Rico Sennrich, Barry Haddow, and Alexandra Birch. Neural machine translation of rare words with subword units. *arXiv preprint arXiv:1508.07909*, 2015. 6
- [52] Karen Simonyan and Andrew Zisserman. Very deep convolutional networks for large-scale image recognition. *arXiv preprint arXiv:1409.1556*, 2014. 5
- [53] Zhicong Tang, Shuyang Gu, Jianmin Bao, Dong Chen, and Fang Wen. Improved vector quantized diffusion models. *arXiv preprint arXiv:2205.16007*, 2022. 3
- [54] Aaron Van den Oord, Nal Kalchbrenner, Lasse Espeholt, Oriol Vinyals, Alex Graves, et al. Conditional image generation with pixelcnn decoders. *NeurIPS*, 29, 2016. 3
- [55] Aaron Van Den Oord, Oriol Vinyals, et al. Neural discrete representation learning. *NeurIPS*, 30, 2017. 1, 3
- [56] Xintao Wang, Liangbin Xie, Chao Dong, and Ying Shan. Real-esrgan: Training real-world blind super-resolution with pure synthetic data. In *ICCV*, pages 1905–1914, 2021. 6
- [57] Zhouxia Wang, Jiawei Zhang, Runjian Chen, Wenping Wang, and Ping Luo. Restoreformer: High-quality blind face restoration from undegraded key-value pairs. In *CVPR*, pages 17512–17521, 2022. 3
- [58] Ronald J Williams and David Zipser. A learning algorithm for continually running fully recurrent neural networks. *Neural computation*, 1(2):270–280, 1989. 4
- [59] Yuxin Wu and Kaiming He. Group normalization. In *ECCV*, pages 3–19, 2018. 12
- [60] Zhenda Xie, Zheng Zhang, Yue Cao, Yutong Lin, Jianmin Bao, Zhuliang Yao, Qi Dai, and Han Hu. Simsim: A simple framework for masked image modeling. In *CVPR*, pages 9653–9663, 2022. 3

- [61] Wilson Yan, Yunzhi Zhang, Pieter Abbeel, and Aravind Srinivas. Videogpt: Video generation using vq-vae and transformers. *arXiv preprint arXiv:2104.10157*, 2021. [3](#)
- [62] Fisher Yu, Ari Seff, Yinda Zhang, Shuran Song, Thomas Funkhouser, and Jianxiong Xiao. Lsun: Construction of a large-scale image dataset using deep learning with humans in the loop. *arXiv preprint arXiv:1506.03365*, 2015. [7](#), [13](#)
- [63] Jiahui Yu, Xin Li, Jing Yu Koh, Han Zhang, Ruoming Pang, James Qin, Alexander Ku, Yuanzhong Xu, Jason Baldridge, and Yonghui Wu. Vector-quantized image modeling with improved vqgan. *arXiv preprint arXiv:2110.04627*, 2021. [1](#), [2](#), [3](#), [6](#), [7](#), [8](#), [12](#)
- [64] Jiahui Yu, Yuanzhong Xu, Jing Yu Koh, Thang Luong, Gungjan Baid, Zirui Wang, Vijay Vasudevan, Alexander Ku, Yinfei Yang, Burcu Karagol Ayan, et al. Scaling autoregressive models for content-rich text-to-image generation. *arXiv preprint arXiv:2206.10789*, 2022. [1](#), [3](#)
- [65] Richard Zhang, Phillip Isola, Alexei A Efros, Eli Shechtman, and Oliver Wang. The unreasonable effectiveness of deep features as a perceptual metric. In *CVPR*, pages 586–595, 2018. [3](#), [5](#)
- [66] Long Zhao, Zizhao Zhang, Ting Chen, Dimitris Metaxas, and Han Zhang. Improved transformer for high-resolution gans. *NeurIPS*, 34:18367–18380, 2021. [4](#), [6](#), [12](#)
- [67] Chuanxia Zheng, Long Tung Vuong, Jianfei Cai, and Dinh Phung. Movq: Modulating quantized vectors for high-fidelity image generation. *arXiv preprint arXiv:2209.09002*, 2022. [2](#), [3](#), [6](#), [7](#)
- [68] Jinghao Zhou, Chen Wei, Huiyu Wang, Wei Shen, Cihang Xie, Alan Yuille, and Tao Kong. ibot: Image bert pre-training with online tokenizer. *arXiv preprint arXiv:2111.07832*, 2021. [3](#), [5](#), [6](#)
- [69] Shangchen Zhou, Kelvin CK Chan, Chongyi Li, and Chen Change Loy. Towards robust blind face restoration with codebook lookup transformer. *arXiv preprint arXiv:2206.11253*, 2022. [3](#)

6. Appendix

In this section, we first present detailed experimental settings in Sec. 6.1. Then we provide more visualization and analysis to understand our observations in Sec. 6.2. More qualitative results of our method are provided in Sec. 6.3. Finally, we discuss the limitation and future work in Sec. 6.4.

Input size	Encoder	Decoder
$f1 : 256 \times 256$	$\frac{\text{Conv, c-128}}{\{\text{Residual Block, 128-c}\} \times 2}$ Downsample Block, 128-c	$\frac{\text{GN-Swish-Conv, c-3}}{\{\text{Residual Block, 128-c}\} \times 2 + \text{B\&D Attn}}$
$f2 : 128 \times 128$	$\frac{\{\text{Residual Block, 128-c}\} \times 2}{\text{Downsample Block, 256-c}}$	$\frac{\text{Upsample Block, c-128}}{\{\text{Residual Block, 256-c}\} \times 2 + \text{B\&D Attn}}$
$f3 : 64 \times 64$	$\frac{\{\text{Residual Block, 256-c}\} \times 2}{\text{Downsample Block, 256-c}}$	$\frac{\text{Upsample Block, c-256}}{\{\text{Residual Block, 256-c}\} \times 2 + \text{B\&D Attn}}$
$f4 : 32 \times 32$	$\frac{\{\text{Residual Block, 256-c}\} \times 2}{\text{Downsample Block, 512-c}}$	$\frac{\text{Upsample Block, c-256}}{\{\text{Residual Block, 256-c}\} \times 2 + \text{B\&D Attn}}$
$f5 : 16 \times 16$	$\frac{\{\text{Residual Block, 512-c}\} \times 4}{\text{GN-Swish-Conv, 256-c}}$	$\frac{\text{Upsample Block, c-256}}{\{\text{Residual Block, 512-c}\} \times 4 + \text{B\&D Attn}}$ Conv, c-512

Table 7. The detailed architecture of SeQ-GAN for 1st phase and 2nd phase learning. The residual block consists of GN [59]-Swish [47]-Conv-GN-Swish-Conv. B&D Attn: interleaved block regional and dilated attention [66]; c: channels; f: compression ratio.

Model	#Params	#Blocks	#Heads	Model Dim	Hidden Dim	Dropout	#Tokens
AR/NAR (Base)	172M	24	16	768	3072	0.1	256
AR/NAR (Large)	305M	24	16	1024	4096	0.1	256

Table 8. The detailed architecture of our autoregressive (AR) and non-autoregressive (NAR) transformers.

6.1. Experimental Setting

Tokenizer learning. As shown in Fig. 7, the architecture of SeQ-GAN follows the implementation of VQGAN. The block regional and dilated attention (B&D Attn) is only added in the 2nd learning phase. The total parameters of SeQ-GAN are 54.5M and 57.9M for 1st and 2nd learning phases, respectively. As suggested in VIT-VQGAN [63], we adopt the style-based discriminator [34] for training SeQ-GAN. The hyperparameters for training SeQ-GAN are summarized in Table. 9.

Generative transformer training. The autoregressive (AR) and non-autoregressive (NAR) transformers share the same architecture, except that the AR transformer has the causal mask on attention. As shown in Table. 8, the base and large model have 172M and 305M parameters, respectively. The detailed training hyperparameters are summarized in Table. 10. In this paper, we adopt the basic sampling technique in VQGAN [18] (*i.e.*, top- p sampling [28]) and MaskGIT [8] (*i.e.*, adjusting sample temperature), but exclude the classifier-free guidance [27] and rejection sampling [48] for simplicity.

Detailed setting for analysis and ablation experiments. Our analysis (*i.e.*, Sec. 3.3 in the manuscript) and ablation experiments (*i.e.*, Sec. 4.4 in the manuscript) are conducted on ImageNet [12]. Compared to the setting for benchmark experiments in Table. 9 and Table. 10, we reduce the batch size of SeQ-GAN learning and generative transformer training to 64. Additionally, we shorten the training iterations of generative transformers to 500,000. The base model with 172M parameters is used for all analysis and ablation experiments.

6.2. More Visualization and Analysis of the Observations

In this section, we provide more visualizations to support our observations. First, consistent with the finding in mc-BEiT [39] that the VQ tokenizer has negligible semantics, we also find the VQ tokenizer is sensitive to human imperceptible low-level changes. Given an image, we add a small Gaussian noise sampled from $\mathcal{N}(\mu, \sigma^2)$, where $\mu = 0$ and $\sigma = 0.01$. As shown in the Fig. 8, although the perceptual change is negligible, the VQ tokenizers quantize the feature into different code indices. This finding motivates us to explore semantics in optimizing VQ tokenizers.

Then, more visualizations are provided to help understand why the objective of semantic compression in tokenizer learning helps the generation. Given the SeQ-GAN with different semantic ratios α , we plot the validation loss curve of its

	ImageNet	FFHQ	Cat	Bedroom	Church
Dataset Statistics					
Training Set	1,281,167	60,000	1,657,266	3,033,042	126,227
Validation Set	50,000	10,000	-	-	-
1st Phase of Tokenizer Learning					
Batch Size	256	64	64	64	32
Iterations	500,000	300,000	26,000	48,000	4,000
Epochs	100	320	1		
Learning Rate	1e-4		5e-5		
LR Decay	Cosine ($end_lr=5e-5$)		-		
Optimizer	Adam ($\beta_1=0.9, \beta_2=0.99$)				
2nd Phase of Tokenizer Learning					
Batch Size	128	32	64	64	32
Iterations	200,000				
Learning Rate	5e-5				
Optimizer	Adam ($\beta_1=0.5, \beta_2=0.9$)				

Table 9. Experimental setting of training SeQ-GAN on ImageNet [12], FFHQ [33], and LSUN [62]-{Cat, Bedroom, Church}.

	ImageNet	FFHQ	Cat	Bedroom	Church
Dataset Statistics					
Training Set	1,281,167	60,000	1,657,266	3,033,042	126,227
Validation Set	50,000	10,000	-	-	-
Autoregressive Transformer (AR)					
Batch Size	256	32	256	256	64
Iterations	1,500,000	500,000			
Optimizer	AdamW ($\beta_1=0.9, \beta_2=0.96, weight_decay=1e-2$)				
Learning Rate	1e-4				
LR Decay	Exponential ($end_lr=5e-6, start_iter = 80,000$)				
Top- p Sampling	0.92	0.98			
Non-Autoregressive Transformer (NAR)					
Batch Size	256	32	256	256	64
Iterations	1,500,000	500,000			
Optimizer	AdamW ($\beta_1=0.9, \beta_2=0.96, weight_decay=1e-2$)				
Learning Rate	1e-4				
LR Decay	Linear ($end_lr=0, start_iter = 50,000$)				
Sampling Temperature	0.45	0.65			

Table 10. Experimental setting of training generative transformers on ImageNet [12], FFHQ [33], and LSUN [62]-{Cat, Bedroom, Church}.

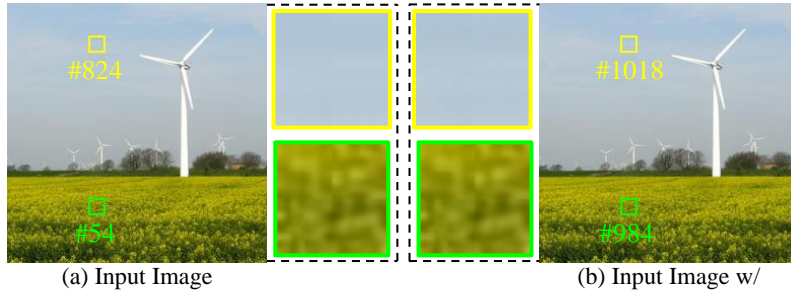


Figure 8. Evidence about VQ quantizers' sensitivity to human imperceptible low-level changes.

corresponding generative transformer training in Fig. 10. Lower validation loss is achieved with a larger semantic ratio α , which shows generative transformers can better model the discrete space constructed by VQ tokenizers with more semantics.

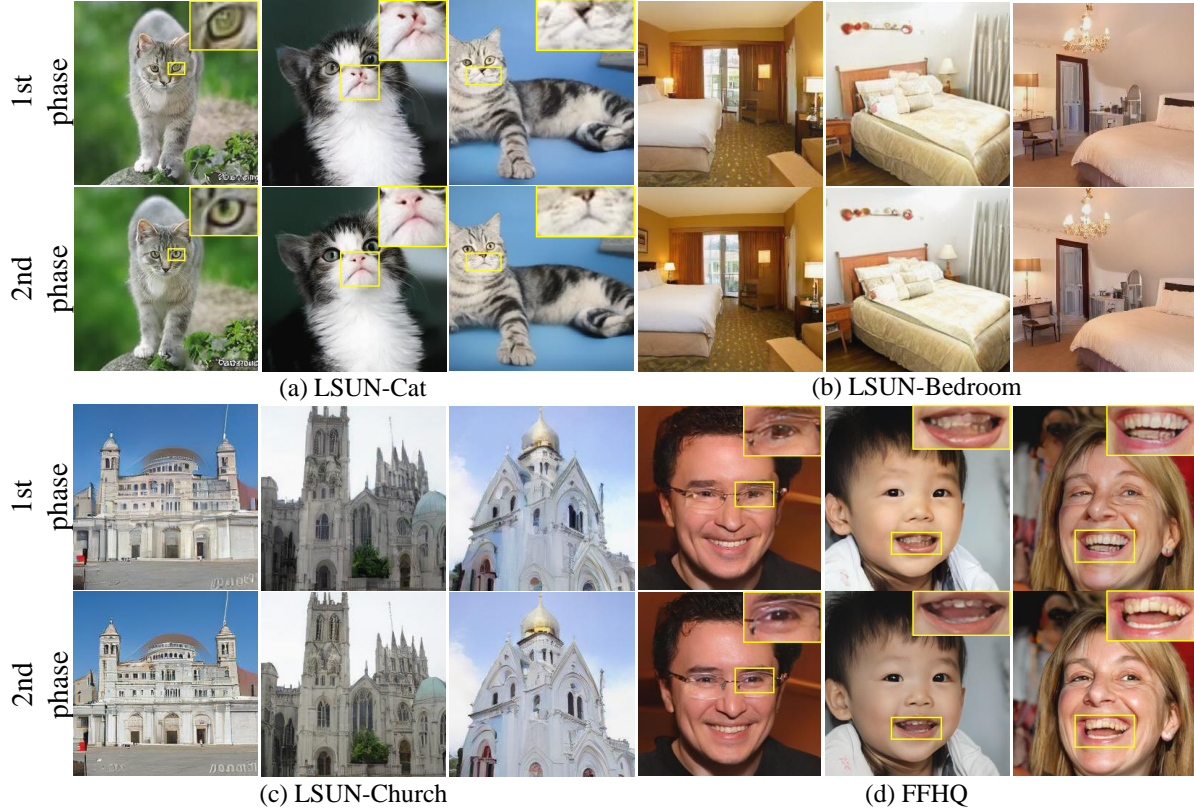


Figure 9. Influence of the 2nd phase tokenizer learning on generation results. (Zoom in for best view.)

Following the proposed visualization pipeline, we visualize the reconstruction and AR prediction of the SeQ-GAN with two different semantic ratios ($\alpha \in \{0, 1\}$). As shown in the Fig. 11, built upon the SeQ-GAN ($\alpha = 1$), the generative transformer can better model each instance (e.g., Row (a-c)), the semantic features (e.g., the cat’s face in Row (d) and the eagle’s beak in Row (e)), and the structure (e.g., the peaked roof in Row (f)). Note that compared to the SeQ-GAN ($\alpha = 0$) in Fig. 11, the reconstruction of the SeQ-GAN ($\alpha = 1$) loses some color fidelity and high-frequency details, which can be restored in our 2nd phase tokenizer learning.

Finally, after the 1st phase of SeQ-GAN ($\alpha = 1$) training, the tokenizer has learned the objective of semantic compression, but loses some details and has spatial distortion (caused by removing shallow layers in $\mathcal{L}_{per}^{\alpha=1}$). The loss of detail in the 1st tokenizer learning can be restored back with our 2nd phase of learning by finetuning an enhanced decoder. As shown in the Fig. 9, we decode the transformer-generated tokens to image space by SeQ-GAN (1st phase) and SeQ-GAN (2nd phase). From the visualization, SeQ-GAN (2nd phase) preserves more details and helps enhance the perceptual quality.

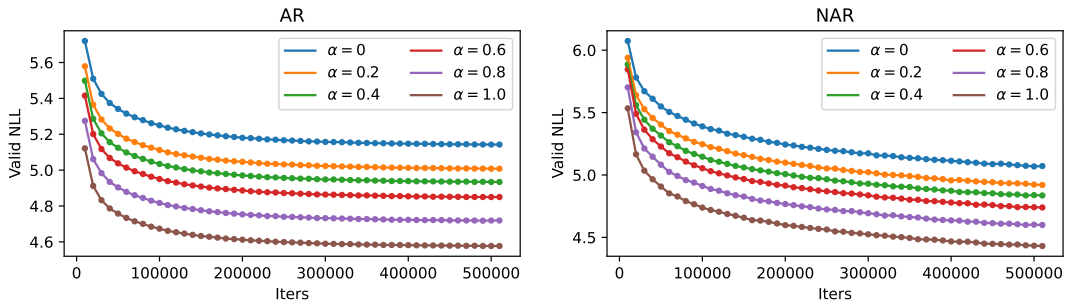


Figure 10. Validation loss curves of generative transformers training on ImageNet. Generative transformers are built upon the SeQ-GAN tokenizers with different semantic ratios (α).

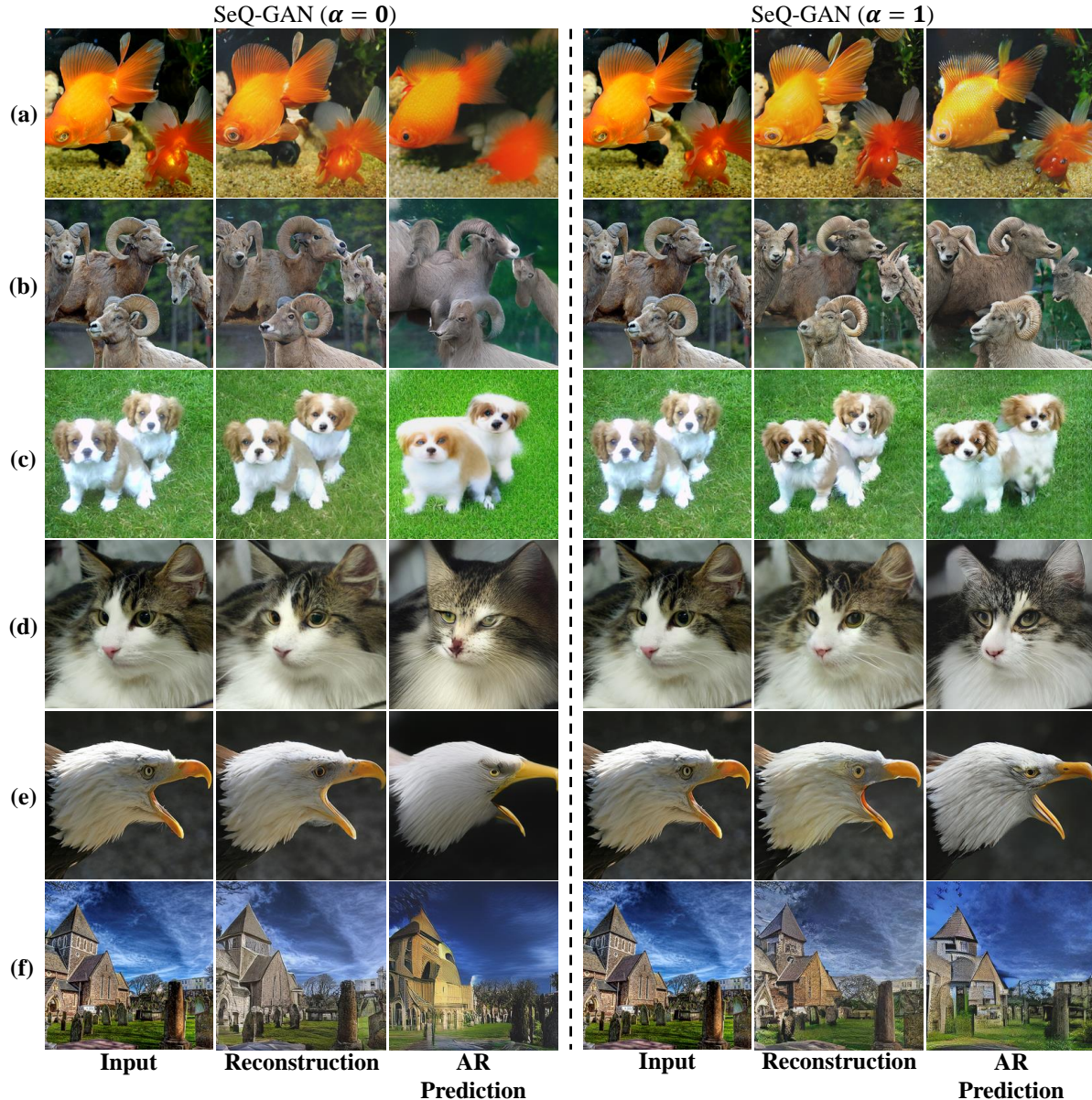


Figure 11. Visual comparison of the influence of SeQ-GAN (with semantic ratios $\alpha \in \{0, 1\}$) on the reconstruction and AR prediction. With the SeQ-GAN ($\alpha = 1$), each instance (e.g., Row (a-c)), the semantic features (e.g., the cat’s face in Row (d) and the eagle’s beak in Row (e)), and the structure (e.g., the peaked roof in Row (f)) are better modeled.

6.3. More Qualitative Results

We provide qualitative comparisons to BigGAN [5], VQGAN [18] and MaskGIT [8] in Fig. 12, Fig. 13 and Fig. 14. For MaskGIT and BigGAN, the samples are extracted from the paper and for VQGAN, we use their pre-generated samples in the official codebase¹. Our SeQ-GAN+NAR produces results with better quality and diversity than previous methods. From the uncurated results in Fig. 15, Fig. 16, Fig. 17 and Fig. 18, our SeQ-GAN+NAR can generate images with high quality and diversity on unconditional image generation.

6.4. Limitation and Future Work

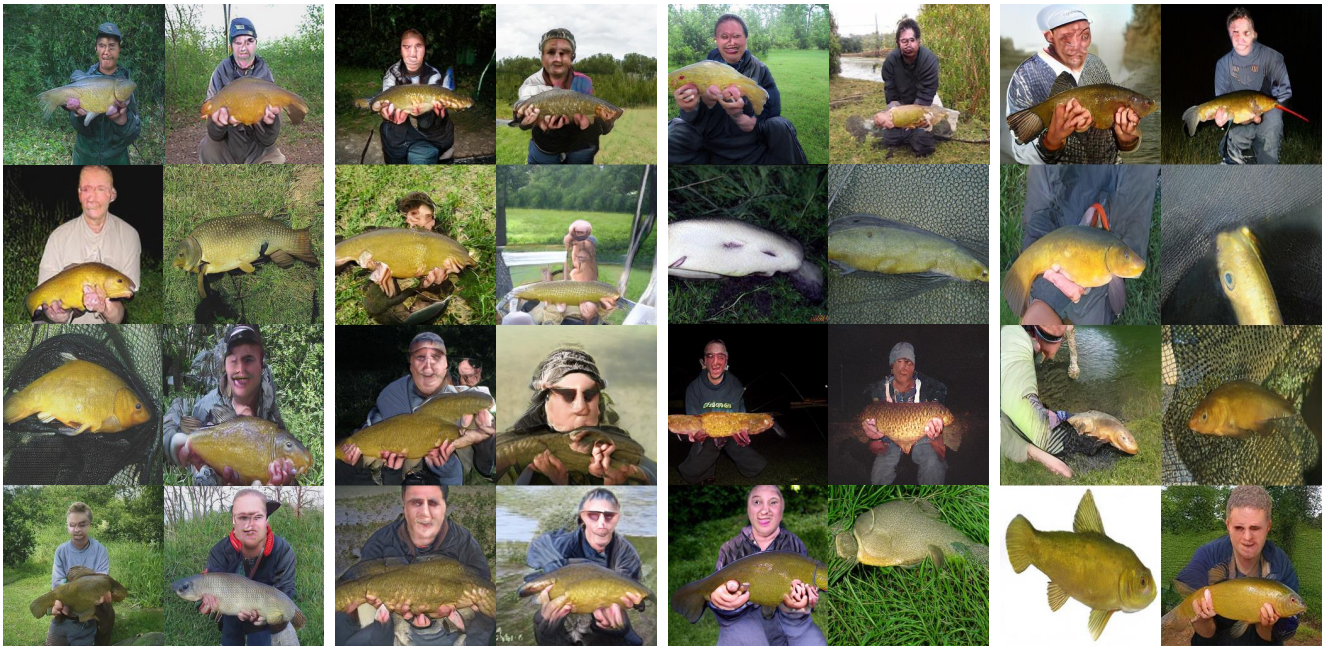
In this work, we want to highlight the importance of semantics in tokenizer learning for visual synthesis. Therefore, we keep the method simple (i.e., controls the semantic ratio by modifying the perceptual loss). Future works on VQ tok-

¹<https://github.com/CompVis/taming-transformers>

enizers may investigate better ways to improve the balance of semantic compression and details preservation. For instance, contrastive learning may be used to make VQ tokenizers learn better semantics compression.

Another limitation inherits from likelihood-based generative models. There are some techniques (*i.e.*, rejection sampling [48] and classifier-free guidance [27]) for likelihood-based generative models to filter out samples with bad shapes and improve sample quality in conditional image generation. However, there are lacking sampling techniques for improving unconditional image generation. As pointed out in [20], classifier-based metrics (*i.e.*, FID) focus more on textures than overall shapes. Therefore, StyleGAN2 finds the perceptual path length (PPL) metric [33] is more related to the shape quality of samples, and they regularize the GAN training to favor lower PPL. Although generative transformers with the SeQ-GAN tokenizer can achieve a better FID than StyleGAN2 in unconditional image generation, some samples have bad overall shapes (see uncurated samples in Fig. 16). Therefore, it is an interesting problem to investigate how to design sample techniques with the idea of PPL for unconditional image generation in likelihood-based generative models.

SeQ-GAN+NAR (FID=4.55) BigGAN-deep (FID=6.95) VQGAN (FID=15.78) MaskGIT (FID=6.18)



SeQ-GAN+NAR (FID=4.55) BigGAN-deep (FID=6.95) VQGAN (FID=15.78) MaskGIT (FID=6.18)

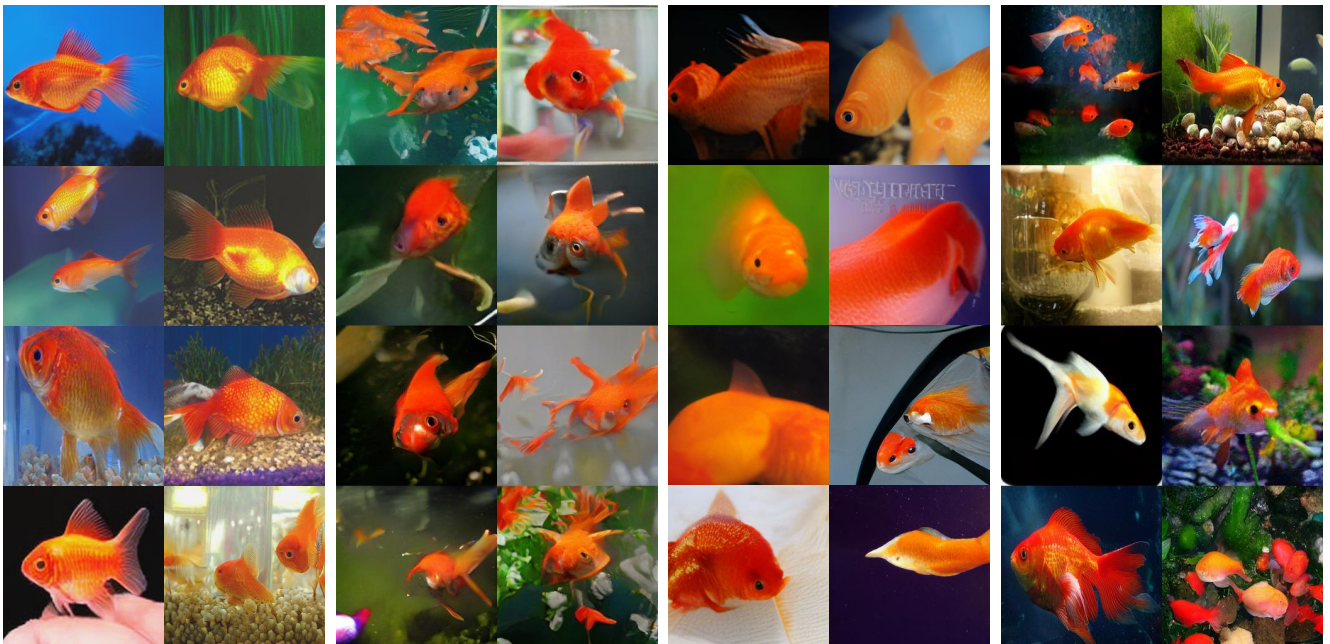


Figure 12. Qualitative comparison with BigGAN [5], VQGAN [18] and MaskGIT [8] on the class 0 (tench) and class 1 (goldfish) of ImageNet [12].

SeQ-GAN+NAR (FID=4.55) BigGAN-deep (FID=6.95) VQGAN (FID=15.78) MaskGIT (FID=6.18)

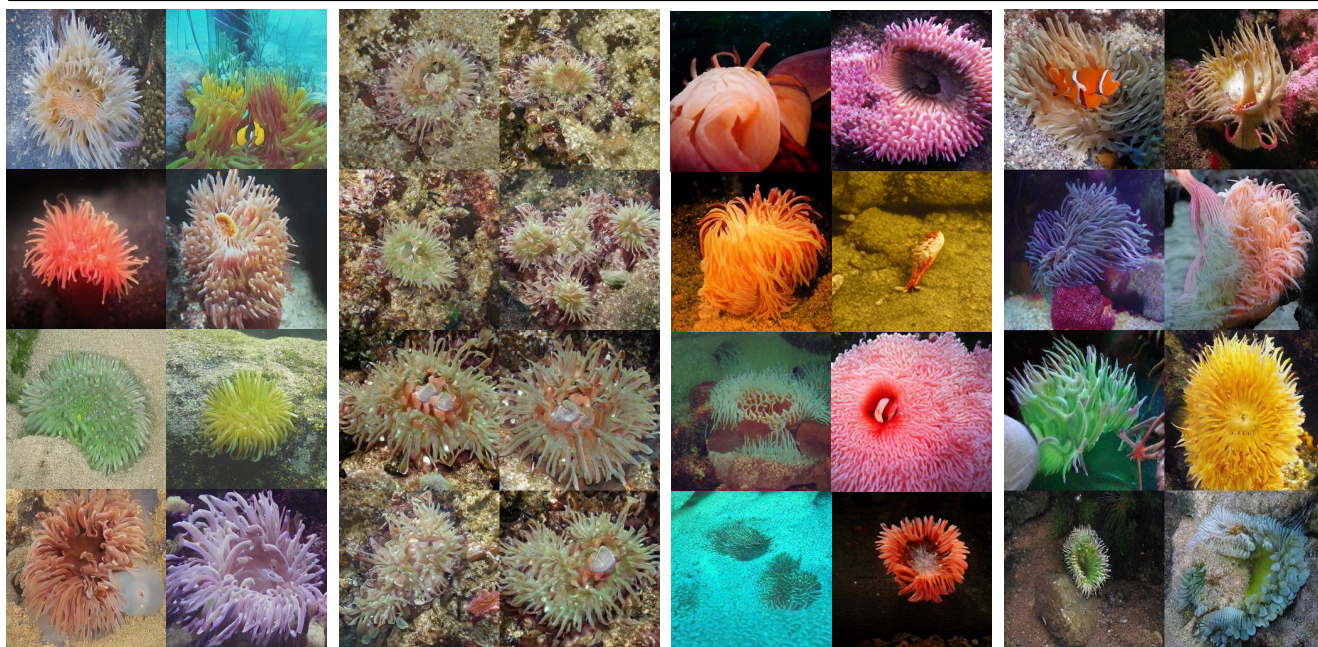


SeQ-GAN+NAR (FID=4.55) BigGAN-deep (FID=6.95) VQGAN (FID=15.78) MaskGIT (FID=6.18)



Figure 13. Qualitative comparison with BigGAN [5], VQGAN [18] and MaskGIT [8] on the class 22 (bald eagle) and class 97 (drake) of ImageNet [12].

SeQ-GAN+NAR (FID=4.55) BigGAN-deep (FID=6.95) VQGAN (FID=15.78) MaskGIT (FID=6.18)



SeQ-GAN+NAR (FID=4.55) BigGAN-deep (FID=6.95) VQGAN (FID=15.78) MaskGIT (FID=6.18)



Figure 14. Qualitative comparison with BigGAN [5], VQGAN [18] and MaskGIT [8] on the class 108 (sea anemone) and class 141 (redshank) of ImageNet [12].



Figure 15. Uncurated set of samples of SeQ-GAN+NAR on 256×256 FFHQ.

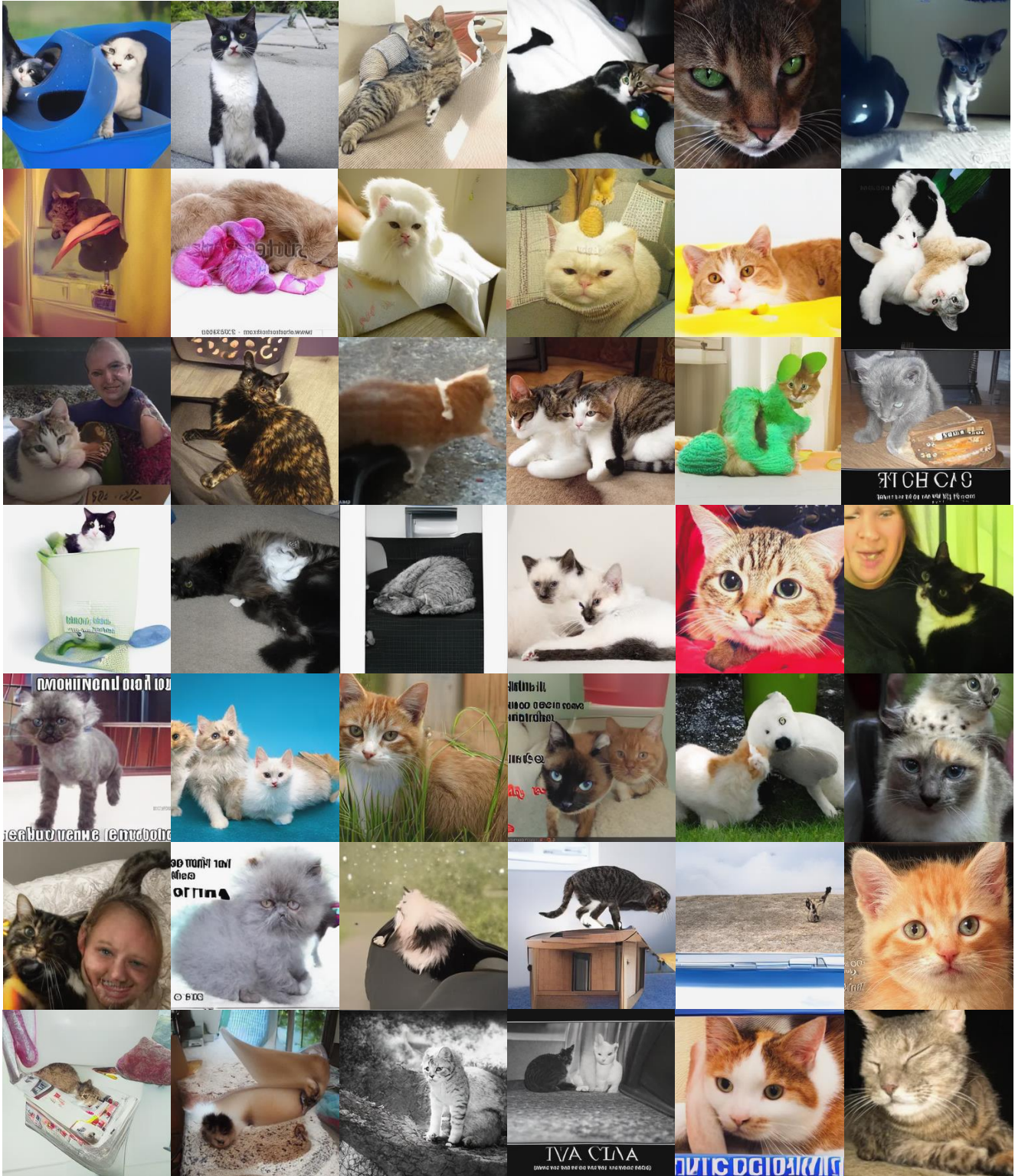


Figure 16. Uncurated set of samples of SeQ-GAN+NAR on 256×256 LSUN cat.



Figure 17. Uncurated set of samples of on 256×256 LSUN church.

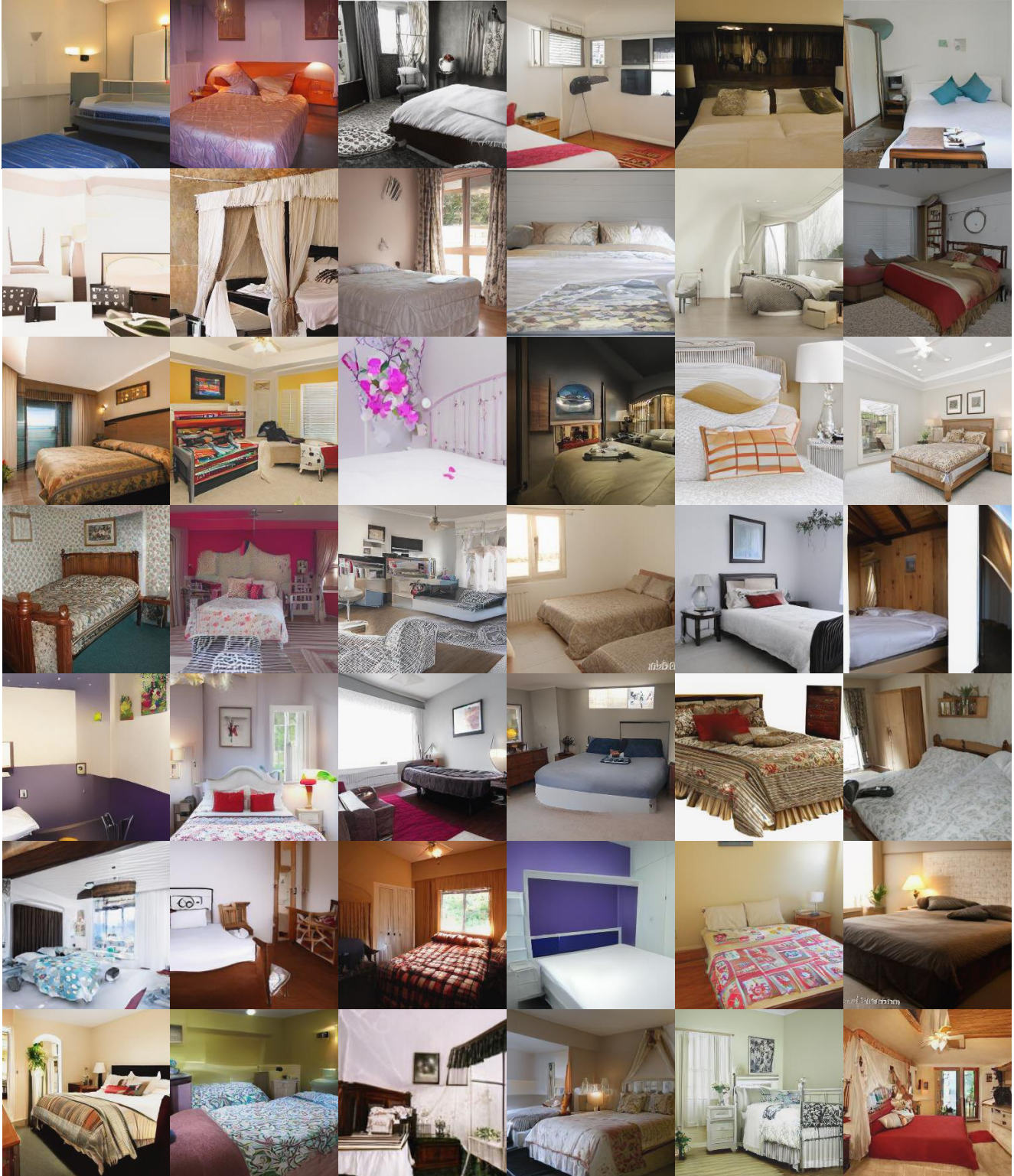


Figure 18. Uncurated set of samples of SeQ-GAN+NAR on 256×256 LSUN bedroom.